Magnetic moments of excited states in the stable chromium isotopes

A. Pakou,* R. Tanczyn, D. Turner,† W. Jan,‡ G. Kumbartzki, N. Benczer-Koller, Xiao-Li Li, Huan Liu, and L. Zamick
Department of Physics, Rutgers University, New Brunswick, New Jersey 08903
(Received 22 May 1987)

The g factors of the first 2_1^+ states in ^{50}Cr and ^{54}Cr have been measured by the perturbed angular correlation/transient field technique. The results, $g(2_1^+, ^{50}\text{Cr}) = +0.45(15)$ and $g(2_1^+, ^{54}\text{Cr}) = +0.53(12)$, are compared to shell model calculations.

I. INTRODUCTION

The Cr isotopes, together with other fp-shell nuclei, are of particular interest to the test of shell model calculations and effective interactions. Moreover, the different structures of ^{52}Cr and the ^{50,54}Cr isotopes, evident from the energy level schemes (Fig. 1), can be specifically tested by g-factor measurements. The g factors of the 2_1^+ states in nuclei with closed ($N=28$ for ^{52}Cr) or nearly closed shells are accessible to measurement only by special techniques because of their short lifetime (few ps). Transient fields are strong enough to provide an appreciable magnetic moment rotation. The technique has been reliably established, but absolute measurements still depend on careful calibrations of the transient field. For Cr isotopes the field is only known via its overall parametrization.[1] However, magnetic moment measurements can still be interpreted reliably within the following context.

(a) The g factors obtained using the Rutgers parametrization[1] for the 2_1^+ states in the neighboring $Z=22$, ^{46,48}Ti isotopes,[2] are in very good agreement with g factors measured independently by recoil in vacuum.[3]

(b) The transient hyperfine field was calibrated at $Z=26$ with the ^{56}Fe 2_1^+ state.[1] The g factor of this state was measured accurately on ^{56}Fe nuclei excited into the 2_1^+ state by nuclear resonance fluorescence[4] or Coulomb excitation[5] and embedded into an iron matrix in which the internal field is well known from Mössbauer absorption experiments.

In addition to the measurements on ^{50}Cr and ^{54}Cr, attempts to determine the g factors of the 2_1^+ state in ^{52}Cr and the $\frac{7}{2}_1^-$ and $\frac{5}{2}_1^-$ states in ^{53}Cr were made. Because of the very low excitation of these states and considerable background, only preliminary results were obtained.

II. EXPERIMENTAL DETAILS

The details of the thin-foil transient field method have been described in previous publications.[6,7] Since the rotation of the magnetic moment is revealed as a rotation of the gamma-ray angular distribution, the experiment was designed to observe the integral rotation of the gamma-ray angular correlation pattern in the transient magnetic field that arises as the corresponding ions move through a polarized iron foil.

Three-layer composite targets were used, whose detailed structures are given in Table I. The iron foil backings for the ^{50,54}Cr targets were made of ^{54}Fe in order to avoid contamination of the ^{50,54}Cr 0.783 and 0.835 MeV gamma rays by the 0.847 MeV line of ^{56}Fe. The targets were placed between the pole pieces of an electromagnet. The experiments were carried out in an external field $H_{\text{ext}}=0.0450$ T at which the ferromagnetic foils were fully saturated. The magnetization of each foil was measured before and after each measurement by a double coil magnetometer.[8] The results are listed in Table I.

The levels of interest were Coulomb excited by a 36 MeV oxygen beam provided by the Rutgers tandem accelerator. The yield was low because of the low atomic number of the projectile and target. However, the particular choice of beam and energy was dictated by conflicting requirements of high recoil velocity and low background considerations.

The gamma rays were detected by four 12.7 cm$\times$ 12.7 cm NaI(Tl) detectors in coincidence with oxygen particles backscattered into a 100 μm Si surface barrier annual detector. Figure 2 shows the coincident particle spectrum. Particle signals were gated by a "fast-slow" coincidence between the time to amplitude

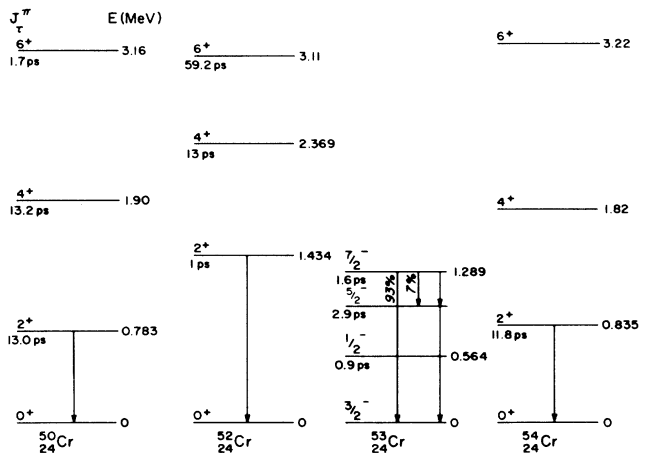

FIG. 1. Energy level diagram of the stable Cr isotopes.

TABLE I. Summary of the target characteristics and of the kinematics of the recoiling Cr nuclei. l is the target thickness, L the thickness of the iron layer, T_f the transit time through the iron foil, $\langle E \rangle_{in}$ and $\langle E \rangle_{out}$ the average energy of the Cr recoil as it enters and leaves the iron foil, and $(v/v_0)_{in}$ and $(v/v_0)_{out}$ the corresponding recoil velocities in units of Bohr velocity $v_0 = e^2/\hbar$.

Nucleus J^π t	E (MeV)	l (mg) cm^2	L (mg) cm^2	A (iron foil)	M (T)	$\langle E \rangle_{in}$ (MeV)	$\langle E \rangle_{out}$ (MeV)	$\left\langle \frac{v}{v_0} \right\rangle_{in}$	$\left\langle \frac{v}{v_0} \right\rangle_{out}$	T_f (psec)
^{50}Cr 2_1^+ 12.99 ps	0.783	0.57	1.28	^{54}Fe	0.1776	20.6	6.6	4.1	2.3	0.24
^{52}Cr 2_1^+ 1.13 ps	1.434	0.70	1.13	nat	0.1565	17.6	6.1	3.7	2.2	0.23
^{53}Cr $\frac{7}{2}^-_1$ 1.58 ps	1.289	0.76	1.30	nat	0.1754	17.7	5.0	3.7	2.0	0.28
^{54}Cr 2_1^+ 11.84 ps	0.835	0.70	1.29	^{54}Fe	0.1709	19.0	5.9	3.8	2.1	0.26

conversion signal and the unanalyzed total particle and gamma-ray pulses. Only gamma rays in coincidence with the high energy backscattered particles were selected by setting an appropriate software window on the particle spectrum [labeled W(Cr) in Fig. 2]. This procedure was mandated by the need to avoid contributions to the gamma-ray spectrum resulting from α-γ coincidences. These alpha particles arise from the ^{12}C(^{16}O,α)^{24}Mg reaction on unavoidable carbon impurities on the target. The arrows labeled α_0, α_2, and α_4 on Fig. 2 indicate the position of the elastic and inelastic alpha peaks. To reduce the carbon buildup on the target, a copper block was placed 0.5 cm behind the target and was maintained at 77 K during the run.

Figure 3 shows the ^{50,54}Cr gamma coincidence spectra.

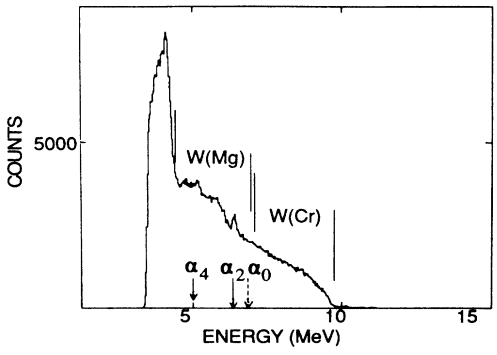

FIG. 2. Spectrum of backscattered oxygen ions gated by the "fast-slow" coincidence gate. The region marked W(Cr) corresponds mostly to oxygen particles backscattered from the Cr target. The region marked W(Mg) contains α's from the reaction ^{12}C(^{16}O,α)^{24}Mg on C contaminants on the target. The arrows at α_0, α_2, and α_4 indicate the position of the elastic and inelastic α peaks.

The spectra of ^{52,53}Cr gamma rays in coincidence with high energy oxygen particles are displayed on Figs. 4(a) and 5(a), respectively, while the spectra obtained with a particle window [labeled W(Mg) on Fig. 2], which encompasses the inelastically backscattered alphas, are shown on Figs. 4(b) and 5(b). The dominance of the

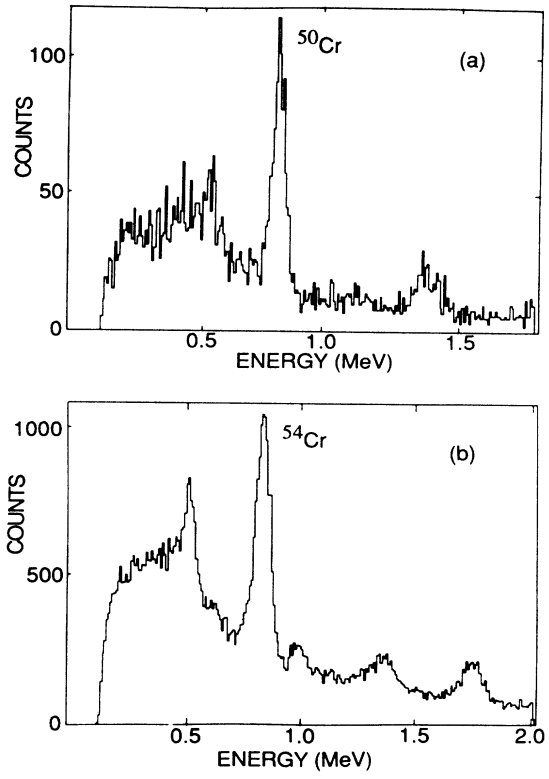

FIG. 3. Gamma-ray spectra in coincidence with particles backscattered from (a) ^{50}Cr and (b) ^{54}Cr targets.

^{24}Mg 1.37 MeV gamma rays is evident. These spectra were corroborated by intensity and angular correlation measurements with Ge(Li) detectors. The peaks appearing at 0.847 MeV correspond to excitation of the 2_1^+ state of ^{56}Fe in the ferromagnetic layer.

The gamma detectors were located 17 cm away from the target at the angle where the slope of the particle-gamma angular correlation is considerable (Figs. 6 and 7); namely $\theta_\gamma = \pm 67.5°$, $\pm 112.5°$ for the even isotopes, and $\theta_\gamma = \pm 60°$, 120° for ^{53}Cr.

The polarizing field was reversed periodically and the change in the coincidence counting rate due to the rotation of the gamma-ray angular correlation was observed. An effect ϵ was deduced from the double ratio of the coincidence yields given by

$$\rho_{ij} = [N_i^{\uparrow}(\theta) N_j^{\downarrow}(\theta) / N_i^{\downarrow}(\theta) N_j^{\uparrow}(\theta)]^{1/2} , \quad (1)$$

$$\rho = (\rho_{14}/\rho_{23})^{1/2} , \quad (2)$$

and

$$\epsilon = (\rho - 1)/(\rho + 1) , \quad (3)$$

where the arrows indicate the direction of the polarizing field. The indices i and j correspond to the appropriate detectors 1, 2, 3, or 4. The rotation $\Delta\theta$ is obtained directly from $\Delta\theta = [\epsilon / S(\theta)]$ where $S(\theta)$ is the logarithmic derivative of the angular correlation function at the angle θ. The cross ratios

$$\rho = (\rho_{13}/\rho_{24})^{1/2} \quad (4)$$

should be unity if no undesired asymmetries appear and were continuously monitored.

III. RESULTS

The experimental rotations are shown in Table II. The g factors are related to the rotations by the expression

$$\Delta\theta = (-\mu_N g/\hbar) \int_0^{T_f} B[v(t)] e^{-t/\tau} dt , \quad (5)$$

where T_f is the transit time through the foil. The Rutgers parametrization[1] was used for the transient hyperfine field $B(v)$,

$$B(v) = 96.7 Z^{1.1} (v/v_0)^{0.45} M \ (\mathrm{T}) , \quad (6)$$

where M is the magnetization of the foil and τ is the mean life of the excited state under study. The integral in Eq. (5) was calculated using stopping powers from Northcliffe and Schilling.[9] The contribution for decays in flight in the ferromagnetic foil was almost zero for all the isotopes except for ^{52}Cr and ^{53}Cr, where the corrections were 12% and 8%, respectively.

The absolute g factors for the 2_1^+ states of ^{50,52,54}Cr

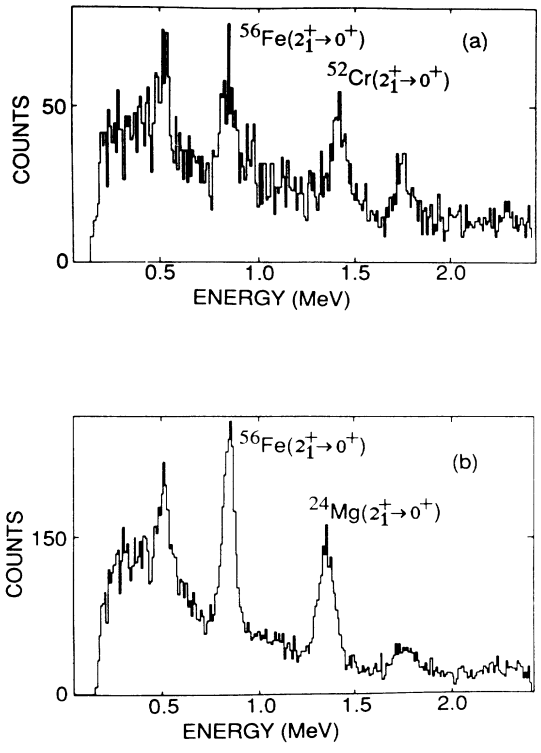

FIG. 4. Gamma-ray spectra of ^{52}Cr generated by coincidence with the particle window corresponding to (a) W(Cr) and (b) W(Mg). The line at 0.847 keV corresponds to the $2_1^+ \rightarrow 0_1^+$ transition in ^{56}Fe in the natural iron foil which is also Coulomb excited in the reaction.

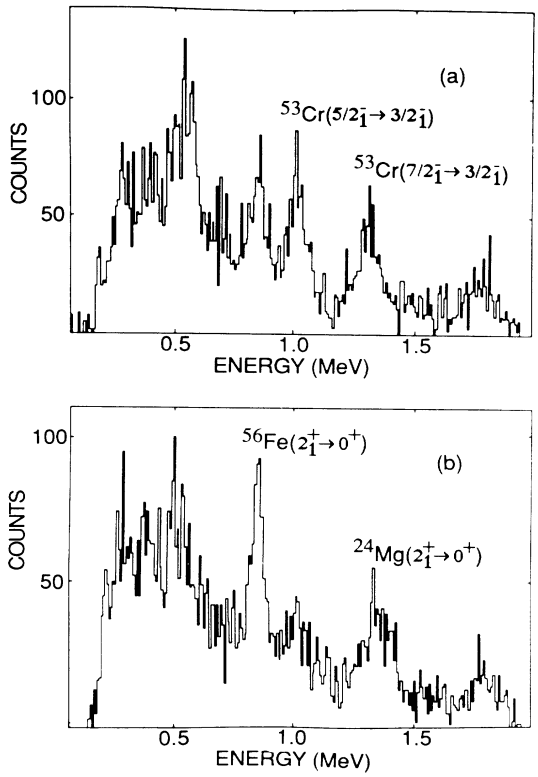

FIG. 5. Gamma-ray spectra of ^{53}Cr generated by coincidence with the particle window corresponding to (a) W(Cr) and (b) W(Mg).

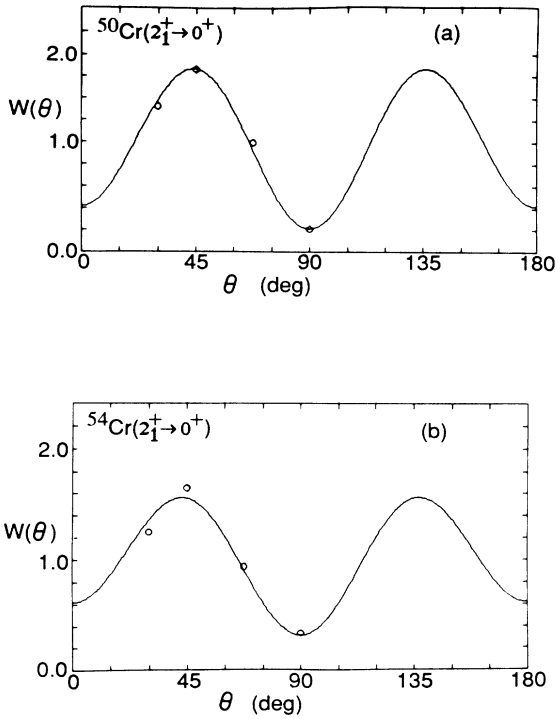

FIG. 6. Particle-gamma angular correlations for the $2_1^+ \rightarrow 0_1^+$ transitions in (a) ^{50}Cr and (b) ^{54}Cr.

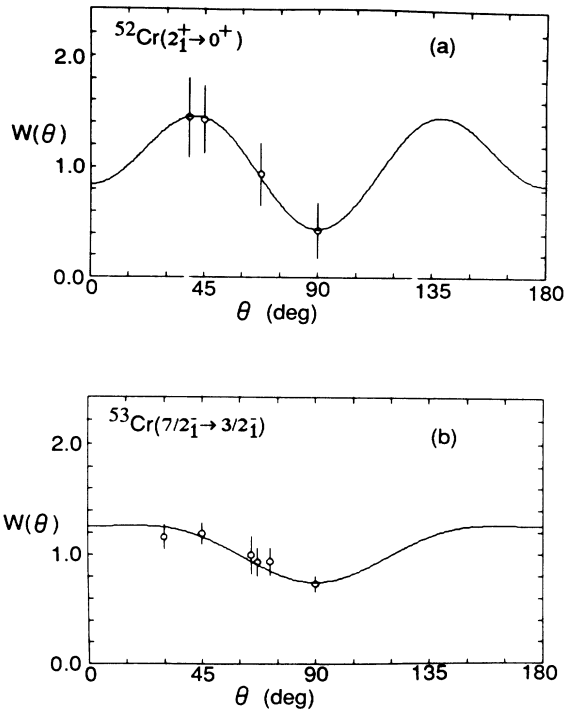

FIG. 7. Particle-gamma angular correlations for the (a) $2_1^+ \rightarrow 0_1^+$ transitions in ^{52}Cr and (b) $\frac{7}{2}^- \rightarrow \frac{3}{2}^-$ transition in ^{53}Cr.

and of the $\frac{7}{2}_1^-$ state of ^{53}Cr have been determined (Table II) and are compared to theoretical predictions in Table III. The large errors in the g factors of the ^{52,53}Cr states are partly due to the weak correlation (^{53}Cr), and partly to the very low excitation probability (^{52,53}Cr). Furthermore, although fairly intense gamma-ray lines were observed for the $\frac{5}{2}^- \rightarrow \frac{3}{2}^-$ transition in ^{53}Cr, the particle-gamma angular correlation was nearly isotropic and no precession could thus be measured.

Measurements on ^{50,54}Cr have previously been performed by Fahlander *et al.*[10] (Table III) by using the static hyperfine magnetic field at Cr ions stopping in thick gadolinium foils. The present results are in good agreement with those measurements. The present data on $g(2_1^+, {}^{52}\text{Cr})$ are also in agreement with recent transient field measurements on ^{52}Cr reported by Stuchbery and collaborators[11] (Table III).

IV. COMPARISON OF EXPERIMENT AND THEORY

Shell model calculations of the low-lying levels of the Cr isotopes have been performed by Mooy and Glaudemans[12] (Table III). Their model space consists of the configurations $f^{-n}r^m$ and $f^{-n-1}r^{m+1}$ (in their notation), where n and m are defined relative to a ^{56}Ni core, f represents the $1f_{7/2}$ shell, and r stands for any of the orbits $2p_{3/2}$, $2p_{1/2}$, and $1f_{5/2}$. The numbers n and m are chosen in an obvious way to yield the lowest possible configuration, for example, $n=1$, $m=3$ for $^{53}_{27}\text{Co}_{31}$; and the second configuration $f^{-n-1}r^{m+1}$ can be regarded as a particle-hole excitation built on the lowest configuration, with the hole restricted to the $f_{7/2}$ shell and the particle to any of the orbits $2p_{3/2}$, $2p_{1/2}$, or $1f_{5/2}$.

In the present paper, the same model space as used by Mooy and Glaudemans[12] was used but a slightly different interaction, FPY, obtained by Yokoyama and Horie[13] with an added modified surface delta interaction, was applied. The only basic difference is that in this work, a wider variety of nuclei was considered in order to establish certain systematics. For example, the g factors of the first excited 2^+ states of the three isotopes ^{46}Ti, ^{48}Ti, and ^{50}Cr were calculated, motivated by the fact that for the lowest configuration for which all nucleons are in the $1f_{7/2}$ shell, the model predicts that $g(^{50}\text{Cr})-g(^{48}\text{Ti}) = g(^{48}\text{Ti})-g(^{46}\text{Ti})$. This result follows from a symmetry which holds only in this very restricted model space: the invariance of the Hamiltonian under the interchange of protons with neutron holes and neutrons with proton holes. It is clearly of interest to see how well this result stands up when the model space is increased to include $f^{-n-1}r^{m+1}$, and more importantly, if it agrees with experiment.

One might question whether the inclusion of only a single-particle hole excitation is adequate to provide a good prediction of the magnetic moments. Unfortunately, the inclusion of all possible configurations in the f-p shell is not possible at this time because of space and time limitations. It is therefore of interest to consider other approaches. Saini and Gunye[14] have considered a

TABLE II. Summary of the angles at which the particle-gamma angular correlations were measured, the slopes of these particle gamma correlations $S(\theta)=(1/W)(dW/d\theta)$, the net precession angles $\Delta\theta$, and the resulting g factors.

Isotope	θ_γ (deg)	S(θ)	$\Delta\theta$ (mrad)	g
^{50}Cr(2_1^+)	±67.5 ±112.5	3.11(8)	−4.8(16)	0.45(15)
^{52}Cr(2_1^+)	±67.5 ±112.5	2.11(80)	−12.8(85)	1.6(11)
^{53}Cr($\frac{7}{2}_1^-$)	±60 ±120	0.73(13)	−8.2(149)	0.8(14)
^{54}Cr(2_1^+)	±67.5 ±112.5	2.65(5)	−5.8(13)	0.53(12)

projected Hartree-Fock calculation which includes band mixing (Table III). This calculation effectively includes the entire f-p shell and therefore could, in principle, yield better results than the restricted shell model calculations derived above. On the other hand, the region of applicability of this particular model is not clear. The underlying picture is that of a deformed nucleus, even though the projection and band mixing yield considerable modifications. The Cr isotopes are generally considered not to be too deformed, especially the semimagic ^{52}Cr. Because of these theoretical uncertainties it is extremely important that experimental measurements be made in order to establish the limits of the validity of the projected Hartree-Fock models.

A. ^{50}Cr

The theoretical value $g(2_1^+)=0.63$ is obtained when all valence nucleons occupy the $f_{7/2}$ shell only, while $g(2_1^+)=0.60$ results when in addition one nucleon is allowed to be excited into the $p_{3/2}$, $f_{5/2}$, or $p_{1/2}$ orbit. The theoretical results are somewhat higher than the experimental moments but consistent with them within the experimental error.

The measurement puts to a severe test the results of single j shell calculations, in particular results concerning the symmetry under the interchange of protons with neutron holes and neutrons with proton holes. Because of this symmetry, which is only valid in the single j shell approximation, the theory predicts that the g factors of the nuclei ^{46}Ti$_{24}$, ^{48}Ti$_{26}$, and ^{50}Cr$_{26}$ will increase linearly with nucleon number A. Moreover, ^{48}Ti is a system with an equal number of protons and neutron holes (two). For this nucleus, the predicted g factor is given by $g=(g_{j\pi}+g_{j\nu})/2=0.554$, where g_j is the Schmidt g factor [for $j=l+\frac{1}{2}$, $g_j=g_l(l/j)+g_s/2j$; for $j=l-\frac{1}{2}$, $g_j=g_l(l+1)/(j+1)-g_s/2(j+1)$]. This result is valid for all states of ^{48}Ti, irrespective of their spin I. Table IV and Fig. 8 display the results of calculations for ^{46}Ti$_{24}$, ^{48}Ti$_{26}$, and ^{50}Cr$_{26}$ for the 2_1^+ states as well as for states of higher angular momentum. The FPY interaction was used.[13] Two calculations were done in each case, one in which all the valence nucleons were in the $f_{7/2}$ shell and one in which one nucleon was allowed to

TABLE III. Comparison of the experimental and theoretical g factors in Cr isotopes.

	g: Experiment						g: Theory			
Nucleus (J^π)	Previous Work	Ref.	Present work	Schmidt limit	Mooy and Glaudemans (Ref. 12)	Saini and Gunye (Ref. 14)	Li, Liu, and Zamick Single j shell	fp shell	Weak-coupling $g_R=1.5$	Weak-coupling $g_R=1.0$
^{50}Cr (2_1^+)	0.59(10)	10	0.45(15)			0.68	0.63[a]	0.60[b]		
^{52}Cr (2_1^+)	1.50(25)	11	1.6(11)	1.51	1.35	1.51				
^{54}Cr (2_1^+)	0.56(10)	10	0.53(12)			0.74	−0.06[c]	0.73[d]		
^{53}Cr ($\frac{3}{2}_1^-$)	−0.316			−1.275	−0.54		−0.98[e]	−0.57[f]		
($\frac{5}{2}_1^-$)				0.547	+1.15		+1.21[e]	1.30[f]	0.47	0.16
($\frac{7}{2}_1^-$)			0.8(14)				0.59[e]	0.64[f]	0.31	0.02

[a] $(f_{7/2})^4_\pi(f_{7/2})^{-2}_\nu$.
[b] $(f_{7/2})^4_\pi(f_{7/2})^{-2}_\nu+(f_{7/2})^3_\pi j_\pi(f_{7/2})^{-2}_\nu+(f_{7/2})^4(f_{7/2})^{-3}_\nu j_\nu$, where $j=(p_{3/2}, f_{5/2}, p_{1/2})$.
[c] $(f_{7/2})^4_\pi(p_{3/2})^2_\nu$.
[d] $(f_{7/2})^4_\pi(p_{3/2}, f_{5/2}, p_{1/2})^2_\nu$.
[e] $(f_{7/2})^4_\pi(p_{3/2}, f_{5/2}, p_{1/2})_\nu$.
[f] $(f_{1/2})^4_\pi j_\nu+(f_{7/2})^3_\pi j_\pi j_\nu+(f_{7/2})^4_\pi(f_{7/2})^{-1}_\nu j_\nu j'_\nu$, where $j,j'=(p_{3/2}, f_{5/2}, p_{1/2})$.

TABLE IV. Calculations of $g(I)$ for ^{46}Ti, ^{48}Ti, and ^{50}Cr with the FPY interaction. j represents the $p_{3/2}$, $f_{5/2}$, or $p_{1/2}$ orbits.

Configuration	^{46}Ti	^{48}Ti	^{50}Cr
	$g(2^+)$		
$f_{7/2}^n$ only	0.476	0.554	0.633
$f_{7/2}^n\bar{1}^1$	0.387	0.281	0.595
	$g(4^+)$		
$f_{7/2}^n$ only	0.153	0.554	0.955
$f_{7/2}^n\bar{1}^1 j$	0.150	0.505	0.899
	$g(6^+)$		
$f_{7/2}^n$ only	0.296	0.554	0.812
$f_{7/2}^n\bar{1}^1$	0.326	0.118	0.804
	$g(8^+)$		
$f_{7/2}^n$ only	0.275	0.554	0.833
$f_{7/2}^n\bar{1}^1 j$	0.387	0.606	0.826
	$g(10^+)$		
$f_{7/2}^n$ only	0.613	0.554	0.495
$f_{7/2}^n\bar{1}^1 j$	0.608	0.627	0.500

go into $p_{3/2}$, $f_{5/2}$, or $p_{1/2}$ orbits. For the single j shell case, the g factors do indeed lie on a straight line. When configuration mixing is permitted, the linearity with A is destroyed, mainly because in the calculation the g factor of ^{48}Ti changes from 0.554 to 0.281. The reason for this

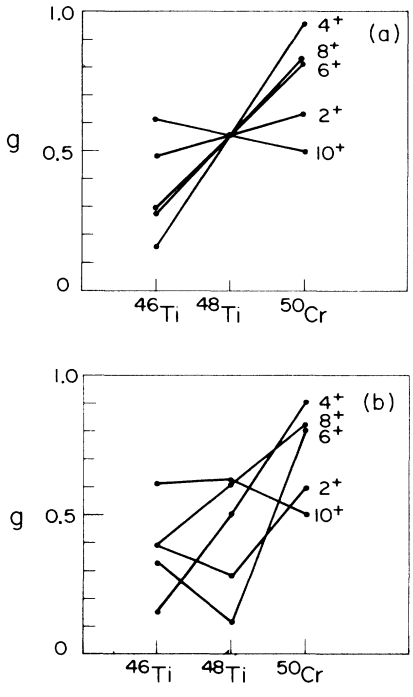

FIG. 8. Theoretical calculations of the spin dependence of the g factors $g(I)$ of the low-lying states of ^{46}Ti, ^{48}Ti, and ^{50}Cr. (a) All valence nucleons are in $f_{7/2}$ shell: $(f_{7/2})^n$. (b) One valence nucleon is allowed to occupy the $(p_{3/2}, f_{5/2}, p_{1/2})$ orbits: $(f_{7/2})^{n-1}(p_{3/2}, f_{5/2}, p_{1/2})$.

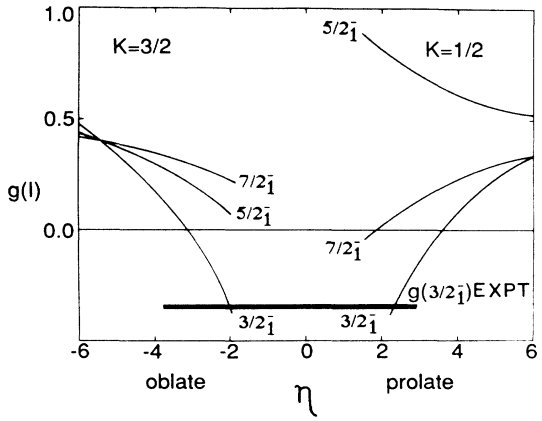

FIG. 9. Theoretical calculations of the g factors of the low-lying states in ^{53}Cr in a model in which the single particle is coupled to a deformed core.

large change is probably due to the fact that, whereas in the single j shell case the g factor is proportional to the isoscalar combination $(g_{j\pi}+g_{j\nu})/2=0.554$, configuration mixing permits an additional contribution proportional to $(g_{j\pi}-g_{j\nu})/2$. This latter term has an unquenched value of 2.2, much larger than the isoscalar combination.

To really test the breakdown of linearity and the contribution of multiple shell occupation, it will be necessary to measure the magnetic moments of the higher spin states in the even Ti and Cr isotopes.

B. ^{54}Cr

It is of interest in this isotope to determine how the protons, mainly in the $f_{7/2}$ shell, and the neutrons in the $p_{3/2}$, $f_{5/2}$, and $p_{1/2}$ shell, compete to produce the observed moment. The measured value of the magnetic moment of the 2_1^+ state is quite different from the shell model calculation for the lowest configuration $(f_{7/2})_\pi^4(p_{3/2})_\nu^2$, $g=-0.06$. However, it should be noted, that whereas a $p_{3/2}$ neutron has a negative g factor, an $f_{5/2}$ neutron has a positive one, $g(f_{5/2})_\nu=0.55$. Thus to obtain the measured rather large positive moment it is necessary to allow two neutrons to roam in the entire $p_{3/2}, f_{5/2}, p_{1/2}$ space. Indeed, when the two neutrons are allowed this freedom, g increase to $+0.73$, and is in closer but not yet good agreement with the experimental value.

C. ^{53}Cr

The measurements of moments in ^{53}Cr also test these various configurations. In Table III the results of calculations with two different shell model configurations are given. The first corresponds to the simplest configuration $(f_{7/2})_\pi^4(p_{3/2}, f_{5/2}, p_{1/2})_\nu$ and the second to configurations where either protons or neutrons can occupy the $p_{3/2}$, $f_{5/2}$, and $p_{1/2}$ orbits.

Also shown in Table III for contrast are weak coupling model values for g for the $I=\frac{5}{2}$ and $I=\frac{7}{2}$ states

$\psi=[p_{3/2},2^+]^I$, $I=\frac{5}{2}$ or $\frac{7}{2}$. The free value of $g(p_{3/2})_\nu=-1.275$ was used together with two different values of g_R for the 2_1^+ vibration of ^{52}Cr, $g_R=1.5$ and $=1$. The weak coupling values are very sensitive to g_R. The g factor obtained for $g_R=1.5$ is closer to the experimentally measured value than is the calculated g factor for $g_R=1$. The results of the weak coupling calculations are quite different from those of the shell model calculation in the restricted model space described above.

The magnetic moments of the $\frac{3}{2}_1^-$, $\frac{5}{2}_1^-$, and $\frac{7}{2}_1^-$ states of ^{53}Cr have also been calculated by coupling the odd neutron within a finite shell model space to a deformed core. The results are graphically displayed on Fig. 9. A determination of the first $\frac{3}{2}_1^-$ ground state and $\frac{7}{2}_1^-$ state moments is not sufficient to distinguish between prolate and oblate shapes. The measured quadrupole moment[15,16] $Q(\frac{3}{2}_1^-)=-0.028\,56$, however, supports an oblate shape. An accurate measurement of the $\frac{5}{2}_1^-$ state could, in principle, establish the shape of Cr^{53} at higher spin, but unfortunately, due to the very small anisotropy of the angular correlation for the $\frac{5}{2}^-\rightarrow\frac{3}{2}^-$ transition, this measurement cannot be carried out.

ACKNOWLEDGMENTS

We would like to thank T. Sommers for his contributions to programming and S. Libonate, A. Piqué, G. Lenner, and D. Barker for their help in running the experiments. A useful communication from B. A. Brown is acknowledged. This work was supported in part by the National Science Foundation and the U. S. Department of Energy.

*Permanent address: Department of Physics, University of Ioannina, Ioannina, Greece.

†Present address: Princeton University, Princeton, NJ 08544.

‡Present address: AT&T Bell Laboratories, Holmdel, NJ 07733.

[1]N. K. B. Shu, D. Melnik, J. M. Brennan, W. Semmler, and N. Benczer-Koller, Phys. Rev. C **21**, 1828 (1980).

[2]$g(2_1^+;\ ^{46}\text{Ti})=0.49(12)$, $g(2_1^+;\ ^{48}\text{Ti})=0.43(19)$; N. K. B. Shu, R. Levy, N. Tsoupas, W. Andrejtscheff, A. Lopez-Garcia, A. Stuchbery, H. H. Bolotin, and N. Benczer-Koller, Hyperfine Interact. **9**, 65 (1981).

[3]$g(2_1^+;\ ^{46}\text{Ti})=0.48(11)$, $g(2_1^+;\ ^{48}\text{Ti})=0.56(11)$; B. J. Murphy, Ph.D. thesis, Oxford, University, (1980).

[4]F. R. Metzger, Nucl. Phys. **27**, 612 (1961).

[5]G. K. Hubler, H. W. Kugel, and D. E. Murnick, Phys. Rev. C **9**, 1954 (1974).

[6]J. M. Brennan, N. Benczer-Koller, M. Hass, and H. T. King, Hyperfine Interact. **4**, 268 (1978).

[7]N. Benczer-Koller, M. Hass, and J. Sak, Annu. Rev. Nucl. Part. Sci. **30**, 53 (1980).

[8]M. Brennan, Ph.D. thesis, Rutgers University, 1978 (unpublished).

[9]L. C. Northcliffe and R. F. Schilling, Nucl. Data **A7**, 233 (1970).

[10]C. Fahlander, K. Johansson, E. Karlsson, and G. Possnert, Nucl. Phys. **A291**, 241 (1977).

[11]A. E. Stuchbery, C. E. Doran, A. P. Byrne, H. H. Bolotin, and G. D. Dracoulis, Hyperfine Interact. **36**, 75 (1987).

[12]R. B. M. Mooy and P. W. M. Glaudemans, Z. Phys. A **312**, 59 (1983).

[13]A. Yokoyama and H. Horie, Phys. Rev. C **31**, 1012 (1985).

[14]S. Saini and M. R. Gunye, Phys. Rev. C **24**, 1694 (1981).

[15]J. A. Thomson, R. P. Scharenberg, W. R. Lutz, and R. D. Larsen, Phys. Rev. C **7**, 1413 (1973).

[16]A. Manoogian and B. Auger, Can. J. Phys. **52**, 1731 (1974).